

Quantum interference between quasi-2D Fermi surface sheets in UTe_2

T. I. Weinberger,^{1,*} Z. Wu,^{1,*} D. E. Graf,² Y. Skourski,³ A. Cabala,⁴ J. Pospíšil,⁴ J. Prokleška,⁴ T. Haidamak,⁴ G. Bastien,⁴ V. Sechovský,⁴ G. G. Lonzarich,¹ M. Vališka,⁴ F. M. Grosche,¹ and A. G. Eaton^{1,†}

¹*Cavendish Laboratory, University of Cambridge,*

JJ Thomson Avenue, Cambridge, CB3 0HE, United Kingdom

²*National High Magnetic Field Laboratory, Tallahassee, Florida, 32310, USA*

³*Hochfeld-Magnetlabor Dresden (HLD-EMFL),*

Helmholtz-Zentrum Dresden-Rossendorf, Dresden, 01328, Germany

⁴*Charles University, Faculty of Mathematics and Physics,*

Department of Condensed Matter Physics, Ke Karlovu 5, Prague 2, 121 16, Czech Republic

(Dated: July 4, 2023)

UTe_2 is a promising spin-triplet superconductor candidate for which high quality samples with long mean free paths have recently become available, thereby enabling quantum oscillation measurements to probe the Fermi surface of this material. The dimensionality of Fermi surface sections of a triplet superconductor can have important implications regarding the topological properties of the superconductivity. For example, UTe_2 has been proposed to possess a chiral superconducting order parameter, which could result in the formation of topologically protected Majorana surface states. Here, we report the observation of oscillatory components in the magnetoconductance of UTe_2 at high magnetic fields. We find that these oscillations are very well described by quantum interference between quasiparticles traversing semiclassical trajectories spanning magnetic breakdown networks. Our observations are fully consistent with a quasi-2D model of this material's Fermi surface based on prior dHvA-effect measurements. Our results indicate that UTe_2 – which exhibits incredibly complex physical properties – possesses a remarkably simple Fermi surface consisting exclusively of two quasi-2D cylindrical sections.

Young's double slit experiment represents a powerful example of the wave-particle duality of photons [1]. A century later Davisson and Germer observed a similar phenomenon involving the quantum mechanical interference of a beam of electrons incident on a crystalline target [2, 3]. In the solid state, superconducting quantum interference devices provide exceptionally accurate measurements of magnetic flux via diffraction-modulated interferometry [4, 5]. For the case of normal metals, the manifestation of quantum interference (QI) effects in the magnetoconductance was first predicted by Shiba and Fukuyama [6], and soon thereafter experimentally realized by Stark and Friedberg in their measurements of the magnetoresistance of magnesium [7]. The concept of the Stark interferometer is premised on interference between semiclassical quasiparticle trajectories across magnetic breakdown (MB) networks connecting separate Fermi surface (FS) sections, yielding oscillations in the conductivity that are periodic in inverse magnetic field strength [8–11].

Since the seminal experiments by Stark and coworkers, quantum interference oscillations (QIOs) have been observed in a variety of materials [12–16] including, in particular, a number of organic metals with quasi-2D (Q2D) FSs consisting primarily of cylindrical pockets [17–24]. Unlike quantum oscillations (QOs) from the dHvA- or SdH-effects, in which phase coherence and Landau quantization of quasiparticles traversing orbits corresponding

to closed FS sections thereby provide a direct measurement of the FS [11], QIOs only yield an indirect probe of the FS, as their frequencies correspond to k -space orbits spanning separate FS sections. Therefore, QIOs are only observed in materials in which the k -space separation of FS sections is sufficiently small for quasiparticles to tunnel between FS sheets in accessible magnetic field strengths [11, 25]. It is important to note that QI is exclusively a kinetic effect and is thus observable in the electrical transport – unlike the dHvA-effect, QIOs do not correspond to an oscillatory component of the free energy, therefore QI effects cannot be observed in bulk thermodynamic properties such as the magnetization [9, 10, 17, 26].

Here, we report the observation of QIOs at high magnetic fields in contactless resistivity measurements of the heavy fermion actinide metal UTe_2 . This material has recently showed promising signs of being a spin-triplet superconductor [27–29] – despite its magnetic groundstate being paramagnetic rather than ferromagnetic, as is the case for the analogous compounds UGe_2 , URhGe and UCoGe [30–32]. Evidence indicating triplet pairing in UTe_2 comes from a number of sources including a negligible change in the NMR Knight shift on cooling through T_c [29, 33] along with anisotropic upper critical fields that far exceed the Pauli limit for singlet pairing in all directions [27, 34–36]. Recent advancements in the growth procedure of single crystal UTe_2 specimens has led to a marked enhancement in crystalline quality, enabling the observation of QOs from the dHvA-effect [37, 38]. The angular profile of the dHvA data is indicative of a relatively simple Q2D FS, consisting of one electron-type

* These authors contributed equally to this work.

† alex.eaton@phy.cam.ac.uk

and one hole-type cylinder, each hosting quasiparticles of heavy effective masses $\sim 40 m_e$ [38].

UTe₂ single crystals were grown by a molten salt flux technique [39] using the methodology detailed in ref. [38]. This technique has been shown to yield high quality specimens of $T_c \approx 2.1$ K with long mean free paths of the order of 100 nm [36–39]. Contactless resistivity measurements were performed in static fields to 41.5 T at the National High Magnetic Field Lab, Tallahassee, Florida, using the tunnel diode oscillator (TDO) technique [40]; similar measurements were obtained in pulsed fields to 70 T at the Hochfeld-Magnetlabor, HZDR, Dresden, using the proximity detector oscillator (PDO) technique [41, 42].

Figure 1 shows the background-subtracted TDO signal (Δf_{TDO}) for magnetic field oriented 8° away from the crystalline c -axis towards the a -axis ($\theta_c = 8^\circ$). The FFT of the Δf_{TDO} data reveals four clear frequency branches, which we label as α - δ . Notably, the FFT spectra at $\theta_c = 8^\circ$ of the TDO signal is very different to the spectra we observed in our prior dHvA study at the same angle (ref. [38]), implying that these are not QOs stemming from the SdH-effect. Furthermore, the amplitude of dHvA QOs diminished by almost an order of magnitude between 19 mK and 200 mK – whereas here the signal is large and very well resolved at 400 mK. These observations indicate that the oscillations in f_{TDO} are likely QIOs not QOs, as QIOs generally correspond to reciprocal space areas constructed from sums and differences between FS sections, and often exhibit effective masses much lower than those of dHvA and SdH QOs [13, 17, 18].

Using our FS model from ref. [38], we illustrate in Figs. 1 & 2 how the frequencies of the α - δ FFT peaks correspond to k -space areas between the cylindrical Fermi sheets, which are centred at the centre and corners of the first Brillouin zone (BZ). Each of these frequency components can thus be well understood as coming from QI between two quasiparticles – one making two orbits around a FS cylinder, and the other traversing a MB network between two cylinders of the same carrier type.

To show this, we consider the generalized theory of MB orbits given by Kaganov and Slutskin [26]. In a magnetic field B the oscillatory component of a kinetic coefficient, such as the electrical conductivity, is composed of combinatory harmonics of the form

$$\sum_{\lambda, \lambda'} \exp[i(\phi_\lambda - \phi_{\lambda'})] = \sum_{\lambda, \lambda'} \exp\left(\frac{i\hbar c}{eB} \mathcal{A}_{\lambda, \lambda'}\right) \quad (1)$$

where λ and λ' are the two semiclassical quasiparticle paths that share a common start and end point, enclosing between them an area in reciprocal space of $\mathcal{A}_{\lambda, \lambda'}$ [43]. The change in phase of the semiclassical quasiparticle wave packet around path λ is simply $\phi_\lambda = \oint_\lambda k_y dk_x$ [18].

Take for example the area \mathcal{A}_β shaded in Fig. 2, which sits at the corner of the first BZ. Writing the area of the hole-type FS cylinder as \mathcal{A}_{h^+} , we can see that the area \mathcal{A}_β is equal to the difference of the areas en-

closed by the paths $\lambda = \text{ACDEA}$ and $\lambda' = \text{ABABA}$ as $\mathcal{A}_{\text{ACDEA}} - \mathcal{A}_{\text{ABABA}} = (2\mathcal{A}_{h^+} + \mathcal{A}_\beta) - 2\mathcal{A}_{h^+} = \mathcal{A}_\beta$. Similarly, areas corresponding to the α , γ and δ frequency components are formed by QI between the quasiparticle trajectories traced in Fig. 1 [44]. The probability of a quasiparticle traversing a path depends on the number of MB tunnelling events (each of probability p) and Bragg reflections (each of probability q) that are contained within the path. Expressing $p = \sqrt{P}$ and $q = i\sqrt{(1-P)}$, where $P = \exp(-B_0/B)$ and B_0 denotes the breakdown field [11, 17, 18, 25, 45], the probabilities for quasiparticles to traverse the paths $\lambda = \text{ACDEA}$ and $\lambda' = \text{ABABA}$, corresponding to the β frequency in Fig. 2, are therefore $q^4 p^4 \exp(i\phi_\lambda)$ and $q^8 \exp(i\phi_{\lambda'})$, respectively. Due to this exponentially suppressed tunnelling probability – which necessitates the application of high magnetic fields – we limit our discussion just to the lowest order relevant networks as depicted in Fig. 1, each of which requires only 4 instances of MB.

By Eqn. 1, we can see that the probability of quasiparticles traversing the paths in Fig. 2 will involve oscillating terms including some proportional to $\cos[\phi_\lambda - \phi_{\lambda'}] = \cos[2\pi(2f_{h^+} + f_\beta - 2f_{h^+})/B] = \cos[2\pi f_\beta/B]$, which will contribute to the (real part of the) conductivity. Furthermore, in the low temperature limit (with phonons frozen out), the temperature dependence of QIOs simply follows the Lifshitz-Kosevich theory [11, 13, 46]. The effective quasiparticle mass is proportional to the dependence of the phase on the electron energy, E_k :

$$\frac{\partial(\phi_\lambda - \phi_{\lambda'})}{\partial E_k} = \frac{2\pi c}{e\hbar B} (m_\lambda^* - m_{\lambda'}^*) \quad (2)$$

where m_i^* denotes the effective mass of path i [13, 18]. Note that it is the difference in the effective masses of the two interfering paths that determines the effective mass of QIOs – thus enabling QIOs to be observed to much higher temperatures than QOs from the dHvA- and SdH-effects [13, 17–19].

Figure 3 shows that the γ and δ frequencies in the QIO spectra of UTe₂ possess effective masses ($\approx 5 m_e$) almost an order of magnitude lower than those reported for dHvA QOs ($\sim 40 m_e$) [37, 38], showing that the subtraction of masses between the two trajectories in Eqn. 2 has almost cancelled out. By contrast, the α and β frequencies are much heavier with masses in the region of 20–35 m_e (Figures 3 and S3). This implies that these MB networks span FS sections with a highly anisotropic distribution of the Fermi velocity, v_F . This is consistent with several experimental [37, 38, 47] and theoretical [48, 49] studies that indicate the hybridization between U f -electrons with the U d -bands and Te p -bands, which provides the dominant contribution to the Q2D FS, can result in significant variations in the effective quasiparticle masses at points around the cylindrical sheets. We note that our uncertainty in m_α^* and m_β^* is considerably larger than for m_γ^* and m_δ^* due to these frequencies only being observable right at the base temperature of

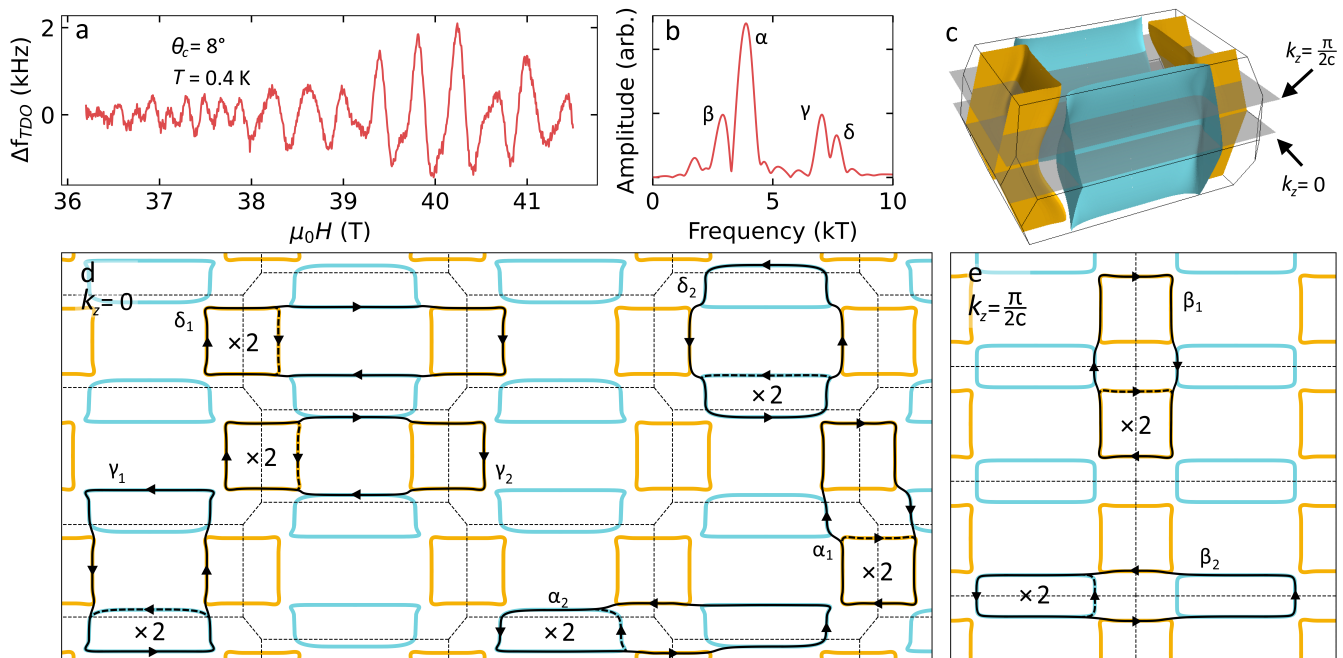


FIG. 1. (a) QIOs in the contactless resistivity of UTe₂ and (b) the corresponding FFT spectra. (c) Our Fermi surface model for UTe₂ adapted from ref. [38], with the planes $k_z = 0$ and $k_z = \frac{\pi}{2c}$ indicated. (d) An extended-zone view, with the c -axis into the page, at $k_z = 0$ and (e) at $k_z = \frac{\pi}{2c}$. QI trajectories enclosing areas that correspond to the QIO frequencies α - δ are indicated; note that each enclosed area α - δ has two distinct MB networks corresponding to it (denoted as $\lambda_{1,2}$).

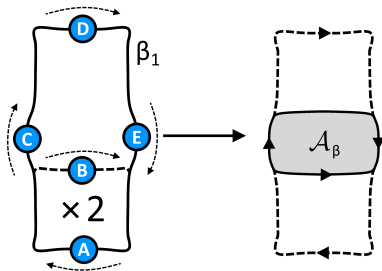


FIG. 2. Schematic of the two semiclassical quasiparticle trajectories that interfere to give the f_β frequency component. The difference in area of the paths ACDEA and ABABA is equal to \mathcal{A}_β , as shown in the text. The frequency components α , γ and δ come from QI between analogous networks, as traced out in Figure 1.

the ³He cryostat used for this measurement, with the uncertainty in temperature dominating the uncertainty in $m_{\alpha,\beta}^*$. Further measurements in the experimentally challenging temperature–field regime of ≤ 200 mK and ≥ 40 T are required to carefully probe the anisotropy of v_F around the FS of UTe₂, and thus to better understand the hybridization of the f , d and p bands.

In principle there is an infinite number of MB networks that could give rise to QIOs. Thus, it is expected that orbits of the type $\mathcal{A}_{ACDEA} - \mathcal{A}_{ABA} = (2\mathcal{A}_{h^+} + \mathcal{A}_\beta) - \mathcal{A}_{h^+} = \mathcal{A}_\beta + \mathcal{A}_{h^+}$ should occur. However, the effective mass associated with these orbits would be greater than

the masses of the hole and electron orbits from which they arise. If in the most simple case we assume that the breakdown orbits of type \mathcal{A}_{ACDEA} have masses of $2m_{h^+/e^-}^* + \epsilon_m$, where ϵ_m is a small difference to account for the fact that quasiparticles are in fact not traversing full FS sheets, then by Eqn. 2 these breakdown orbits need to interfere with two full FS sheet orbits to produce oscillations of $m^* = \epsilon_m$. By comparison, orbits of the type $\mathcal{A}_{ACDEA} - \mathcal{A}_{ABA}$ would instead have masses of $m^* = m_{h^+/e^-}^* + \epsilon_m$ and as such would be too heavy to observe at ³He temperatures.

Figure 4 shows the evolution of QIO frequency with magnetic field tilt angle, and compares with the prediction from our Q2D FS model (in panel c). Although this is only a crude approximation of the expected QIO frequency profile, we find remarkably good agreement between our FS model adapted from ref. [38] and the QIOs we observe in TDO measurements. This result gives strong confidence that the FS of UTe₂ is very well described by our Q2D model.

Our discussion so far has focussed on field aligned coaxially to the FS cylinders (along c), and at inclination angles close to c . Figure 5 shows that for field oriented along the a -axis, two additional frequencies $f_\iota = 220$ T and $f_\kappa = 4.5$ kT are observed. Again, the enclosed areas of these MB networks correspond very well to our Q2D FS model (Fig. 5f). The low frequency ι oscillations for field along a are of considerable amplitude, and are clearly observable in the raw TDO signal without background subtrac-

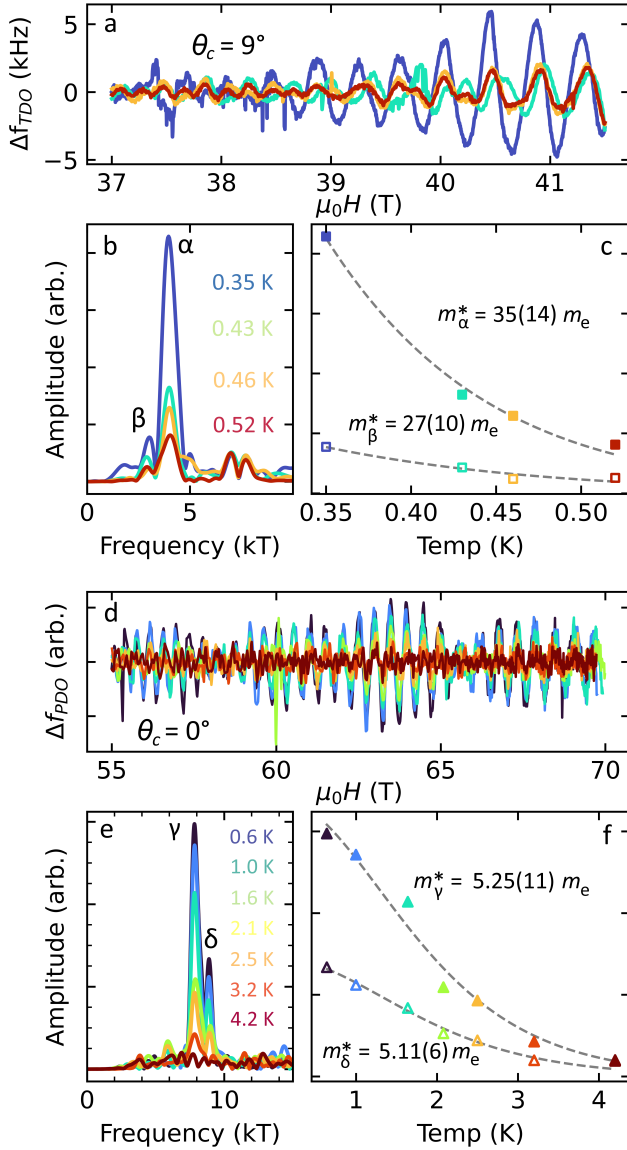


FIG. 3. QIOs, FFTs, and effective masses for (a-c) steady field measurements focussing on the α and β components, and (b-e) higher temperature pulsed field measurements focussing on γ and δ . The effective masses m_γ^* and m_δ^* are markedly lower than those observed in dHvA-effect measurements [37, 38].

tion (Fig. 5a). Along the a -axis ι again corresponds to a QIO, whereas κ is consistent with a conventional MB orbit, which may explain its small amplitude as well its observation only directly at the a -axis.

We note that a similar study of oscillations in the TDO signal of UTe_2 at high fields was recently reported [50]. For $H \parallel a$ ref. [50] reports an oscillatory frequency of 223 T, in very good agreement with the 200 T ι orbit we observe at this field orientation (Fig. 5). However, rather than being of a QI origin, the authors of ref. [50] interpreted the observed oscillatory waveform to com-

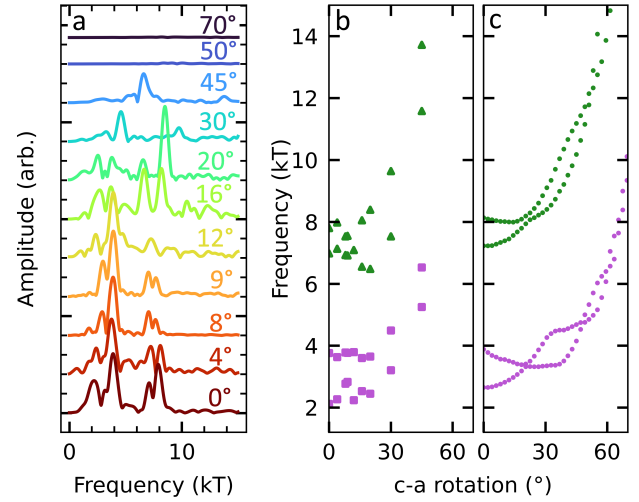


FIG. 4. (a) Evolution of FFT spectra as a function of magnetic field tilt angle away from the c -axis. (b) Frequency versus angle for the α and β branches (in purple) and the γ and δ branches (in green). (c) The expectation of the angular frequency profile corresponding to the areas $\mathcal{A}_{\alpha,\beta,\gamma,\delta}$ computed from our FS model depicted in Fig. 1. Surprisingly good correspondence between model prediction and experimental measurement is observed, given the simplicity of the model assumptions (given in the Supplementary Materials).

prise QOs from the SdH-effect caused by the presence of light 3D FS pocket(s). The distinction between Q2D and 3D FS dimensionality in the case of UTe_2 is important, as any 3D pockets could have significant implications regarding the topological properties of the putatively spin-triplet superconductivity [51, 52].

However, in our measurements we do not observe any indication of the presence of a 3D FS pocket. Fig. 5b shows the evolution of Δf_{TDO} as the field is tilted away from a towards c . For magnetic field oriented along the a -axis we observe low frequency large amplitude oscillations, in good agreement with the raw data presented in ref. [50]. A large oscillatory component is still visible 9° away from a ; however, after a rotation of 20° (to $\theta_c = 70^\circ$) no oscillations are observed within the resolution of the measurement. This is inconsistent with this frequency branch coming from SdH-effect QOs due to a 3D pocket; however, this behavior is consistent with a QI interpretation of the oscillatory origin, as the ι trajectory is only possible close to a . Furthermore, no slow oscillations at these tilt angles have been reported in prior dHvA measurements by the field modulation [37] or torque magnetometry [38] techniques – they appear only to be observed in the electrical conductivity, again consistent with a QI origin.

The stark difference in the effective masses of the α , β and γ , δ components implies a strong anisotropy of $v_F(\mathbf{k})$. In our recent study of dHvA QOs in UTe_2 we observed two-fold effective mass variations along the measured fre-

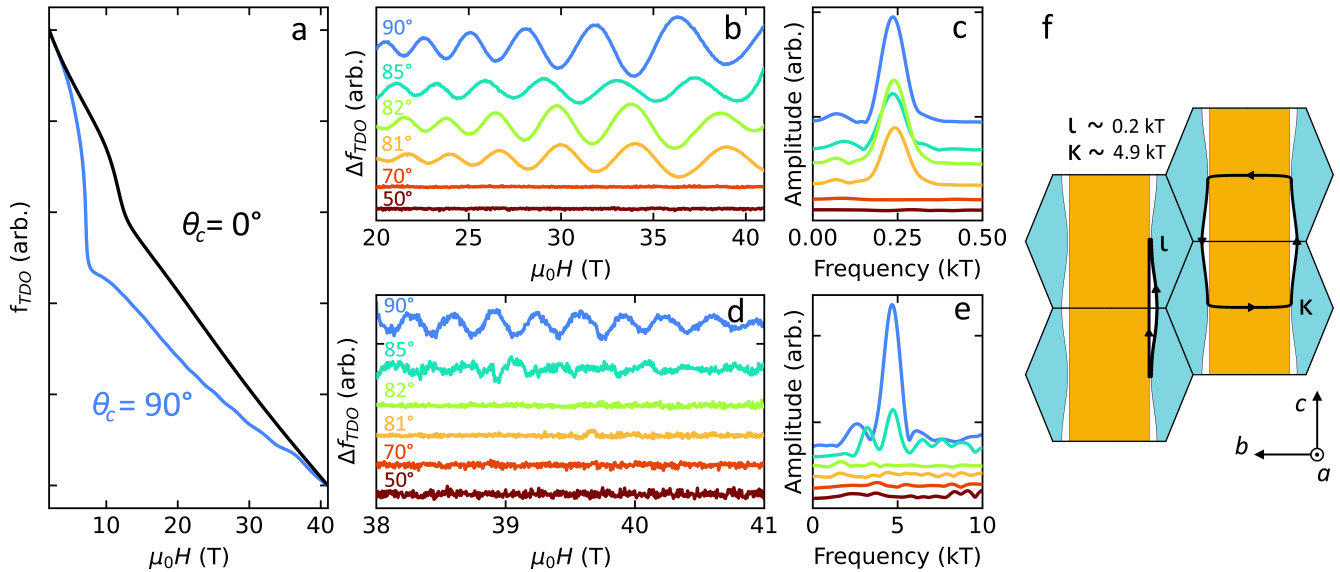


FIG. 5. (a) Raw TDO signal for field oriented along the c -axis ($\theta_c = 0^\circ$) and along the a -axis ($\theta_c = 90^\circ$). (b) QIOs at θ_c angles as indicated over 20-41.5 T and (c) their corresponding FFTs. (d) High frequency oscillations at $\theta_c = 90^\circ$ that are quickly suppressed by rotation away from the a -axis. (e) FFTs of the curves in panel d. Only the data at $\theta_c = 90^\circ$ has a resolvable frequency component above the noise floor of the measurement. (f) A side-view of the cylindrical sheets of our Q2D FS model (compared to the axial-view given in Fig. 1). The trajectories ι and κ are identified, which enclose areas with very good correspondence to the oscillatory frequencies observed for magnetic field orientated along the a -axis.

quency branches under rotation away from the c -axis [38]. In order to attain such a variation, this implies a significant anisotropy of $v_F(k_z)$, which in turn could account for the large difference in effective masses of the QIOs. Such a variation in effective mass likely stems from substantial hybridization between U d -bands and Te p -bands, which are the main contributors to the Q2D FS sheets [49], and a spectral f -electron band sitting just above the Fermi level. This band has been detected in ARPES measurements, in which a significant spectral weight was observed at the Z-point of the BZ [47]. Models of UTe₂ that include the presence of such a band [48, 49] show that the effect of the U f -electrons hybridizing with U d -bands is to compress them in energy, effectively increasing their band mass. A similar effect, albeit less pronounced, would also be relevant for the Te p -band. It is therefore likely that v_F is lowest (and thus m^* is highest) at the regions of the FS cylinders that are closest to the Z point, as here the spectral contribution of the f -electrons is largest and thus the hybridization with them will be the greatest.

In summary, we measured the contactless resistivity of UTe₂ to high applied magnetic field strengths. We observed oscillatory components that are well explained by quantum interference between semiclassical quasiparticle trajectories spanning magnetic breakdown networks. We find that the quantum interference frequencies correspond very well to a quasi-2D model of the UTe₂ Fermi surface. Our observations give no indication of the presence of any 3D Fermi surface pockets.

ACKNOWLEDGMENTS

We are grateful to N.R. Cooper, D.V. Chichinadze, D. Shaffer, A.J. Hickey, H. Liu, P. Coleman, J. Chen, C.K. de Podesta, O.P. Squire, T. Helm, and especially A.F. Bangura for stimulating discussions. We thank T.J. Brumm and S.T. Hannahs for technical advice and assistance. This project was supported by the EPSRC of the UK (grant no. EP/X011992/1). A portion of this work was performed at the National High Magnetic Field Laboratory, which is supported by National Science Foundation Cooperative Agreement No. DMR-1644779* and the State of Florida. We acknowledge support of the HLD at HZDR, a member of the European Magnetic Field Laboratory (EMFL). The EMFL also supported dual-access to facilities at MGML, Charles University, Prague, under the European Union's Horizon 2020 research and innovation programme through the ISABEL project (No. 871106). Crystal growth and characterization were performed in MGML (mgml.eu), which is supported within the program of Czech Research Infrastructures (project no. LM2023065). We acknowledge financial support by the Czech Science Foundation (GACR), project No. 22-22322S. T.I.W. acknowledges support from EPSRC studentship EP/R513180/1. Z.W. acknowledges studentship support from the Cambridge Trust (www.cambridgetrust.org) and the Chinese Scholarship Council (www.chinesescholarshipcouncil.com). T.I.W. and A.G.E. acknowledge support from QuantEmX grants from ICAM and the Gordon and Betty Moore Foundation through Grants GBMF5305 & GBMF9616. A.G.E.

acknowledges support from the Henry Royce Institute for Advanced Materials through the Equipment Access Scheme enabling access to the Advanced Materi-

als Characterisation Suite at Cambridge, grant numbers EP/P024947/1, EP/M000524/1 & EP/R00661X/1; and from Sidney Sussex College (University of Cambridge).

-
- [1] T. Young, I. The Bakerian Lecture. Experiments and calculations relative to physical optics, *Philos. Trans. R. Soc.* **94**, 1 (1804).
- [2] C. Davisson and L. H. Germer, The scattering of electrons by a single crystal of nickel, *Nature* **119**, 558 (1927).
- [3] C. Davisson and L. H. Germer, Diffraction of Electrons by a Crystal of Nickel, *Phys. Rev.* **30**, 705 (1927).
- [4] B. D. Josephson, Possible new effects in superconductive tunnelling, *Phys. Lett.* **1**, 251 (1962).
- [5] J. E. Mercereau, *Superconductivity*, Vol. 1 (Marcel Dekker, New York, 1969) edited by R. D. Parks.
- [6] H. Shiba and H. Fukuyama, A Quantum Theory of Galvanomagnetic Effect in Metals with Magnetic Breakdown. I, *J. Phys. Soc. Jpn.* **26**, 910 (1969).
- [7] R. Stark and C. Friedberg, Quantum interference of electron waves in a normal metal, *Phys. Rev. Lett.* **26**, 556 (1971).
- [8] R. Stark and C. Friedberg, Interfering electron quantum states in ultrapure magnesium, *J. Low Temp. Phys.* **14**, 111 (1974).
- [9] R. Stark and R. Reifenberger, Quantitative theory for the quantum interference effect in the transverse magnetoresistance of pure magnesium, *J. Low Temp. Phys.* **26**, 763 (1977).
- [10] D. Morrison and R. Stark, Two-lifetime model calculations of the quantum interference dominated transverse magnetoresistance of magnesium, *J. Low Temp. Phys.* **45**, 531 (1981).
- [11] D. Shoenberg, *Magnetic Oscillations in Metals* (Cambridge University Press, Cambridge, UK, 1984).
- [12] S. Uji, T. Terashima, H. Aoki, J. S. Brooks, M. Tokumoto, S. Takasaki, J. Yamada, and H. Anzai, Rapid oscillations in the organic conductor (TMTSF)₂CIO₄, *Phys. Rev. B* **53**, 14399 (1996).
- [13] N. Harrison, R. G. Goodrich, J. J. Vuillemin, Z. Fisk, and D. G. Rickel, Quantum Interference in LaB₆, *Phys. Rev. Lett.* **80**, 4498 (1998).
- [14] N. Harrison, D. W. Hall, R. G. Goodrich, J. J. Vuillemin, and Z. Fisk, Quantum Interference in the Spin-Polarized Heavy Fermion Compound CeB₆: Evidence for Topological Deformation of the Fermi Surface in Strong Magnetic Fields, *Phys. Rev. Lett.* **81**, 870 (1998).
- [15] D. Graf, J. S. Brooks, E. S. Choi, M. Almeida, R. T. Henriques, J. C. Dias, and S. Uji, Quantum interference in the quasi-one-dimensional organic conductor (Per)₂Au(mnt)₂, *Phys. Rev. B* **75**, 245101 (2007).
- [16] N. L. Nair, M.-E. Boulanger, F. Laliberté, S. Griffin, S. Channa, A. Legros, W. Tabis, C. Proust, J. Neaton, L. Taillefer, and J. G. Analytis, Signatures of possible surface states in TaAs, *Phys. Rev. B* **102**, 075402 (2020).
- [17] N. Harrison, J. Caulfield, J. Singleton, P. Reinders, F. Herlach, W. Hayes, M. Kurmoo, and P. Day, Magnetic breakdown and quantum interference in the quasi-two-dimensional superconductor κ -(BEDT-TTF)₂Cu(NCS)₂ in high magnetic fields, *J. Phys. Condens. Matter* **8**, 5415 (1996).
- [18] M. V. Kartsovnik, G. Y. Logvenov, T. Ishiguro, W. Biberacher, H. Anzai, and N. D. Kushch, Direct Observation of the Magnetic-Breakdown Induced Quantum Interference in the Quasi-Two-Dimensional Organic Metal κ -(BEDT-TTF)₂Cu(NCS)₂, *Phys. Rev. Lett.* **77**, 2530 (1996).
- [19] J. Singleton, Studies of quasi-two-dimensional organic conductors based on BEDT-TTF using high magnetic fields, *Rep. Prog. Phys.* **63**, 1111 (2000).
- [20] J. M. Schrama, J. Singleton, R. S. Edwards, A. Ardavan, E. Rzepniewski, R. Harris, P. Goy, M. Gross, J. Schlueter, M. Kurmoo, *et al.*, Millimetre-wave measurements of the bulk magnetoconductivity of anisotropic metals: application to the organic superconductors κ -(BEDT-TTF)₂Cu(NCS)₂ and β'' -(BEDT-TTF)₂SF₅CH₂CF₂SO₃ (BEDT-TTF≡bis(ethylene-dithio)tetrathiafulvalene), *J. Phys. Condens. Matter* **13**, 2235 (2001).
- [21] C. Proust, A. Audouard, L. Brossard, S. Pesotskii, R. Lyubovskii, and R. Lyubovskaya, Competing types of quantum oscillations in the two-dimensional organic conductor (BEDT-TTF)₈Hg₄Cl₁₂(C₆H₅Cl)₂, *Phys. Rev. B* **65**, 155106 (2002).
- [22] M. V. Kartsovnik, High Magnetic Fields: A Tool for Studying Electronic Properties of Layered Organic Metals, *Chem. Rev.* **104**, 5737 (2004).
- [23] A. Audouard, D. Vignolles, C. Proust, L. Brossard, M. Nardone, E. Haanappel, S. Pesotskii, R. Lyubovskii, and R. Lyubovskaya, Magnetic oscillations in a two-dimensional network of coupled orbits, *Physica B Condens. Matter* **346**, 377 (2004).
- [24] R. Lyubovskii, S. Pesotskii, E. Zhilyaeva, A. Flakina, and R. Lyubovskaya, The Electron Structure of Metallic Layers in the Quasi-Two-Dimensional Dual-Layered Organic Metal (BETS)₄HgBr₄(C₆H₄Cl₂), *Tech. Phys. Lett.* **45**, 407 (2019).
- [25] R. G. Chambers, Magnetic breakdown in real metals, *Proc. Phys. Soc.* **88**, 701 (1966).
- [26] M.I. Kaganov and A.A. Slutskin, Coherent magnetic breakdown, *Phys. Rep.* **98**, 189 (1983).
- [27] S. Ran, C. Eckberg, Q. P. Ding, Y. Furukawa, T. Metz, S. R. Saha, I. L. Liu, M. Zic, H. Kim, J. Paglione, and N. P. Butch, Nearly ferromagnetic spin-triplet superconductivity, *Science* **365**, 684 (2019).
- [28] S. Ran, I. L. Liu, Y. S. Eo, D. J. Campbell, P. M. Neves, W. T. Fuhrman, S. R. Saha, C. Eckberg, H. Kim, D. Graf, F. Balakirev, J. Singleton, J. Paglione, and N. P. Butch, Extreme magnetic field-boosted superconductivity, *Nat. Phys.* **15**, 1250 (2019).
- [29] D. Aoki, J. P. Brison, J. Flouquet, K. Ishida, G. Knebel, Y. Tokunaga, and Y. Yanase, Unconventional superconductivity in UTe₂, *J. Phys. Condens. Matter* **34**, 243002 (2022).
- [30] S. S. Saxena, P. Agarwal, K. Ahilan, F. M. Grosche, R. K. W. Haselwimmer, M. J. Steiner, E. Pugh, I. R. Walker, S. R. Julian, P. Monthoux, G. G. Lonzarich, A. Huxley,

- I. Sheikin, D. Braithwaite, and J. Flouquet, Superconductivity on the border of itinerant-electron ferromagnetism in UGe₂, *Nature* **406**, 587 (2000).
- [31] D. Aoki, A. Huxley, E. Ressouche, D. Braithwaite, J. Flouquet, J. P. Brison, E. Lhotel, and C. Paulsen, Coexistence of superconductivity and ferromagnetism in URhGe, *Nature* **413**, 613 (2001).
- [32] N. T. Huy, A. Gasparini, D. E. de Nijs, Y. Huang, J. C. P. Klaasse, T. Gortenmulder, A. de Visser, A. Hamann, T. Görlach, and H. v. Löhneysen, Superconductivity on the Border of Weak Itinerant Ferromagnetism in UCoGe, *Phys. Rev. Lett.* **99**, 067006 (2007).
- [33] H. Matsumura, H. Fujibayashi, K. Kinjo, S. Kitagawa, K. Ishida, Y. Tokunaga, H. Sakai, S. Kambe, A. Nakamura, Y. Shimizu, *et al.*, Large Reduction in the a -axis Knight Shift on UTe₂ with $T_c = 2.1$ K, *J. Phys. Soc. Jpn.* **92**, 063701 (2023).
- [34] B. Chandrasekhar, A note on the maximum critical field of high-field superconductors, *Appl. Phys. Lett.* **1**, 7 (1962).
- [35] A. M. Clogston, Upper Limit for the Critical Field in Hard Superconductors, *Phys. Rev. Lett.* **9**, 266 (1962).
- [36] Z. Wu, T. I. Weinberger, J. Chen, A. Cabala, D. V. Chichinadze, D. Shaffer, J. Pospisil, J. Prokleška, T. Haidamak, G. Bastien, V. Sechovsky, A. J. Hickey, M. J. Mancera-Ugarte, S. Benjamin, D. E. Graf, Y. Skourski, G. G. Lonzarich, M. Valiska, F. M. Grosche, and A. G. Eaton, Enhanced triplet superconductivity in next generation ultraclean UTe₂ (2023), [arXiv:2305.19033](https://arxiv.org/abs/2305.19033).
- [37] D. Aoki, S. Hironori, O. Petr, T. Yoshifumi, I. Jun, Y. Youichi, H. Hisatomo, N. Ai, L. Dexin, H. Yoshiya, S. Yusei, K. Georg, F. Jacques, and H. Yoshinori, First Observation of the de Haas–van Alphen Effect and Fermi Surfaces in the Unconventional Superconductor UTe₂, *J. Phys. Soc. Jpn.* **91**, 083704 (2022).
- [38] A. G. Eaton, T. I. Weinberger, N. J. M. Popiel, Z. Wu, A. J. Hickey, A. Cabala, J. Pospíšil, J. Prokleška, T. N. Haidamak, G. Bastien, P. Opletal, H. Sakai, Y. Haga, R. Nowell, S. M. Benjamin, V. Sechovský, G. G. Lonzarich, F. M. Grosche, and M. Vališka, Quasi-2D Fermi surface in the anomalous superconductor UTe₂ (2023), [arXiv:2302.04758](https://arxiv.org/abs/2302.04758).
- [39] H. Sakai, P. Opletal, Y. Tokiwa, E. Yamamoto, Y. Tokunaga, S. Kambe, and Y. Haga, Single crystal growth of superconducting UTe₂ by molten salt flux method, *Phys. Rev. Materials* **6**, 073401 (2022).
- [40] C. T. Van Degrift, Tunnel diode oscillator for 0.001 ppm measurements at low temperatures, *Rev. Sci. Instr.* **46**, 599 (2008).
- [41] M. M. Altarawneh, C. H. Mielke, and J. S. Brooks, Proximity detector circuits: An alternative to tunnel diode oscillators for contactless measurements in pulsed magnetic field environments, *Rev. Sci. Instr.* **80**, 066104 (2009).
- [42] S. Ghannadzadeh, M. Coak, I. Franke, P. Goddard, J. Singleton, and J. L. Manson, Measurement of magnetic susceptibility in pulsed magnetic fields using a proximity detector oscillator, *Rev. Sci. Instr.* **82**, 113902 (2011).
- [43] Note that the calculation of $\mathcal{A}_{\lambda, \lambda'}$ is dependent on both the number and the direction of the trajectories included in λ and λ' .
- [44] Each of $\mathcal{A}_\lambda = \{\mathcal{A}_\alpha, \mathcal{A}_\beta, \mathcal{A}_\gamma, \mathcal{A}_\delta\}$ have two distinct QI paths corresponding to them, each requiring only 4 instances of MB, which we label as $\lambda_{1,2}$.
- [45] L. M. Falicov and H. Stachowiak, Theory of the de Haas–van Alphen Effect in a System of Coupled Orbits. Application to Magnesium, *Phys. Rev.* **147**, 505 (1966).
- [46] I. M. Lifshitz and A. M. Kosevich, Dokl. Akad. Nauk. SSSR **96**, 963 (1954).
- [47] L. Miao, S. Liu, Y. Xu, E. C. Kotta, C.-J. Kang, S. Ran, J. Paglione, G. Kotliar, N. P. Butch, J. D. Denlinger, and L. A. Wray, Low Energy Band Structure and Symmetries of UTe₂ from Angle-Resolved Photoemission Spectroscopy, *Phys. Rev. Lett.* **124**, 076401 (2020).
- [48] J. Ishizuka and Y. Yanase, Periodic Anderson model for magnetism and superconductivity in UTe₂, *Phys. Rev. B* **103**, 094504 (2021).
- [49] D. Shaffer and D. V. Chichinadze, Chiral superconductivity in UTe₂ via emergent C_4 symmetry and spin-orbit coupling, *Phys. Rev. B* **106**, 014502 (2022).
- [50] C. Broyles, Z. Rehfuss, H. Siddiquee, K. Zheng, Y. Le, M. Nikolo, D. Graf, J. Singleton, and S. Ran, Revealing a 3D Fermi Surface and Electron-Hole Tunneling in UTe₂ with Quantum Oscillations (2023), [arXiv:2303.09050](https://arxiv.org/abs/2303.09050).
- [51] H. C. Choi, S. H. Lee, and B.-J. Yang, Correlated normal state fermiology and topological superconductivity in UTe₂ (2022), [arXiv:2206.04876](https://arxiv.org/abs/2206.04876).
- [52] M. Sato and Y. Ando, Topological superconductors: a review, *Rep. Prog. Phys.* **80**, 076501 (2017).

Supplementary materials for: *Quantum interference between quasi-2D Fermi surface sheets in UTe₂*

1 SAMPLE CALIBRATION AND MEASUREMENT

High quality MSF-grown single crystal UTe₂ samples were selected for quantum oscillation studies, each of which exhibited singular superconducting transitions in specific heat capacity measurements, with $T_c > 1.95$ K. In order to perform contactless resistivity measurements via either the TDO or PDO technique, samples were placed on top of planar coils (Figure S1a).

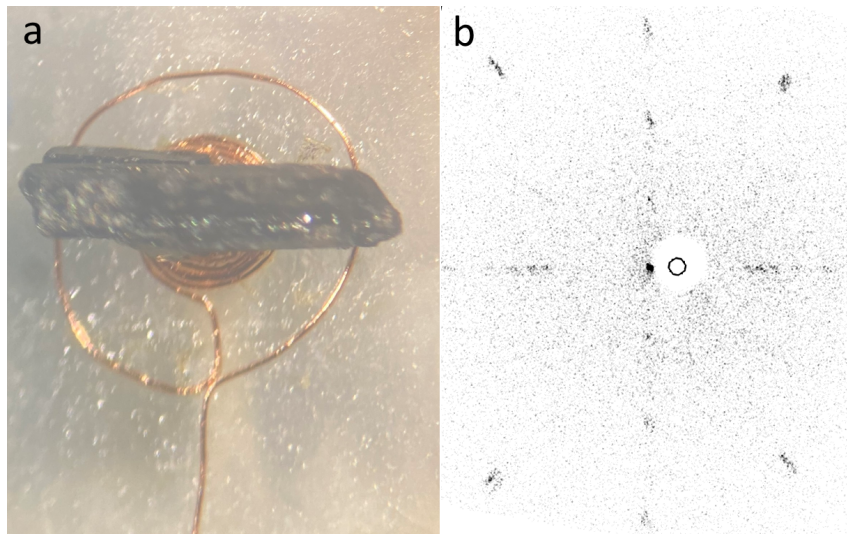


Figure S1: (a) Sample of high quality UTe₂ mounted on a planar coil. (b) Lauegram of the sample in panel (a) taken once it had been mounted on the coil. The measured spectrum is in good agreement with the expected c -axis spectrum, with no extraneous peaks observed.

The use of planar coils provides two benefits:

1. Firstly, this allows for measurements of a single sample in both pulsed-field and dc-field measurements, without having to change the coil. In pulsed fields a planar coil is desirable, as a compensation loop is easily wound, in order to minimise dB/dt through the coil as the field is rapidly increased and decreased thereby minimising the pick-up of the field itself (and thus maximising the sensitivity to the sample) [?].

- Secondly, using a planar coil allows a Lauegram of the sample to be taken after it has been mounted, ensuring good knowledge of the sample alignment (Figure S1b).

2 LIFSHITZ-KOSEVICH ANALYSIS FOR $H \parallel [001]$

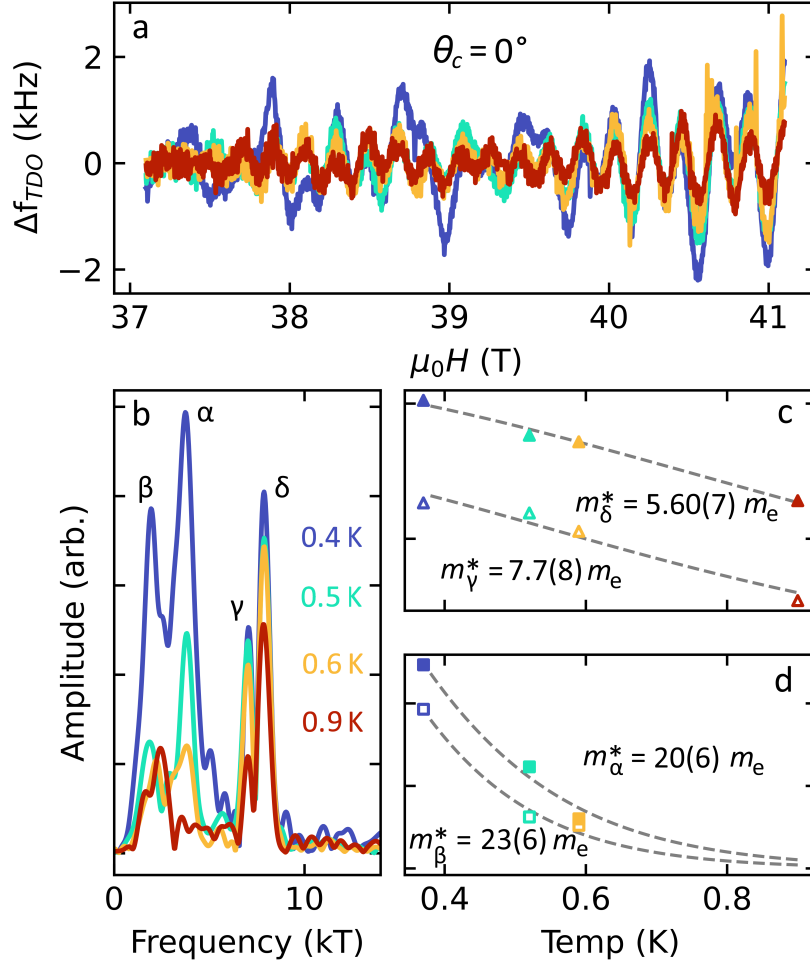


Figure S2: (a) Background-subtracted contactless resistivity of UTe₂ as measured along the c -axis in the field range 37–41 T at incremental temperatures as indicated. (b) The associated FFTs showing all four distinct frequencies at 2.4 kT, 3.9 kT, 7.9 kT, and 8.4 kT corresponding to the α , β , γ , and δ frequencies, respectively. Increasing temperature rapidly suppresses the α and β frequencies, whereas the γ and δ are more resistant to increasing temperatures due to their lighter effective masses. (c-d) The Lifshitz-Kosevich temperature dependence of γ and δ shows that these higher frequencies are lighter in effective mass whereas the α and β are substantially heavier.

3 VARIABLE-FIELD STUDY

For magnetic field applied along the c -axis, the similarity in frequency expected for the α frequency, and the SdH signal expected for the actual cylindrical Fermi surface sheets [?], complicates the analysis of the TDO signal. By our Fermi surface model of the possible QI orbits in UTe_2 , the α frequency is predicted to be at ≈ 3.8 kT, whereas the cyclotron orbits around the (degenerate) hole and electron sheets will produce a SdH frequency of ≈ 3.4 kT.

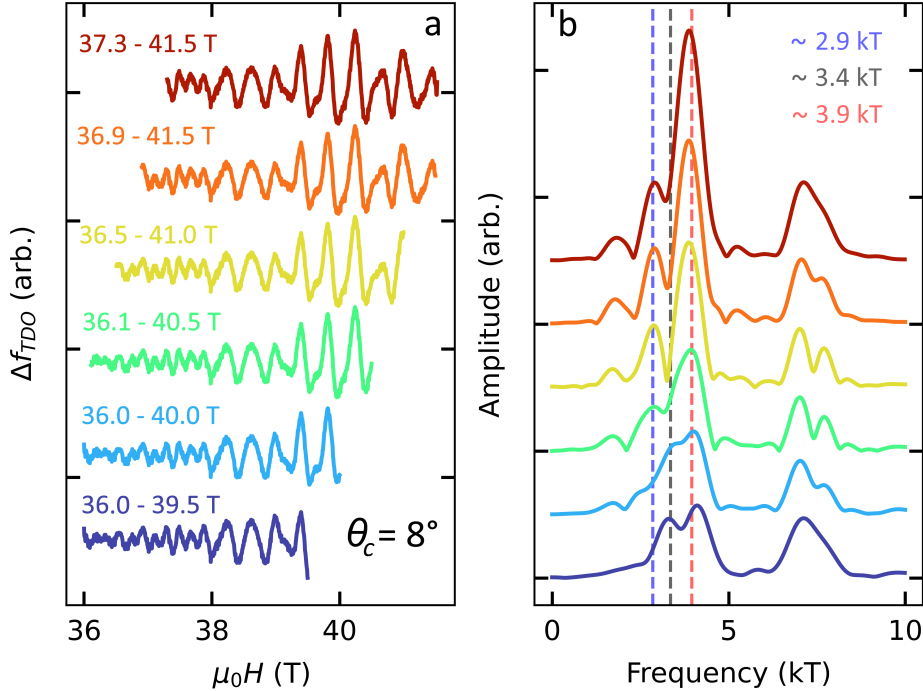


Figure S3: (a) Background-subtracted contactless resistivity signal over different field windows as indicated, showing the onset of different oscillation frequencies. (b) The associated FFTs show that at 36 T a high frequency component is present, whereas the lower frequency oscillations only become well resolved above 39.5 T. In this lower field range there appears to be two frequencies, one at ≈ 3.9 kT corresponding to a QIO, whereas there is also a clear peak at 3.4 kT which would be in good agreement with the conventional SdH QO orbit. As the field window is increased to around 41 T a new oscillatory frequency is observable at 2.9 kT, while the 3.9 kT frequency is enhanced at higher field ranges. This 2.9 kT oscillation is in good agreement with a predicted QIO frequency, and is also enhanced at increasing field ranges. Conversely, the 3.4 kT frequency component does not increase in amplitude as rapidly at high field.

Data was analysed with a variable field range in order to determine the evolution of the frequency spectrum as a function of field, to delineate between oscillatory components that may be from conventional SdH QOs, and those that can only be explained as being QIOs (Figure S3).

Close to the c -axis, in the lowest field window of 36.0–39.5 T, the high-frequency γ and δ frequencies onset at ≈ 36 T, whereas the α QIO at 3.9 kT only begins to be observable at ≈ 38 T. In this field range, the β frequency is not observed. Alongside these QIOs, in the lowest field window, an FFT peak at 3.4 kT is clearly visible. This frequency is in good agreement with the dominant QO frequency branch previously observed in dHvA measurements [?].

Once the field has increased above ≈ 40 T, another QIO becomes observable at ≈ 2.9 kT, corresponding to the predicted β frequency. In this range, the 3.4 kT QO peak is only observable as a broadening of the 3.9 kT QIO. For increasingly higher field windows, the intensity of each peak in the QIO spectrum is enhanced whereas the 3.4 kT peak intensity does not increase, and becomes swamped by the QIOs.

The simultaneous measurement of all four predicted QIOs, as well as a frequency component that likely corresponds to a SdH QO orbit directly corresponding to the Fermi surface at lower fields, indicates that by limiting our analysis to the highest field ranges, the resolved oscillation spectrum corresponds to peaks from QIOs only. Therefore, this analysis provides good confidence that our discussion presented in the main text is relevant to the QIO spectrum of UTe_2 , and thereby provides valuable information pertaining to the Fermi surface geometry of this material.

4 DETAILS OF QUANTUM INTERFERENCE ORBIT FREQUENCY CALCULATIONS

The effective area for each QIO can be determined according to Fig. 1 of the main text; the areas are effectively equal to the smallest loops enclosed by the outer surface of each cylinder. To model the QIOs upon rotating away from the c -axis, we start from the Fermi surface model of our earlier dHvA-effect QO study of UTe_2 [?]. Using this model, we define slicing planes between each cylinder along the directions of minimal k -space separation. Example bounding cylinders for the α and δ frequencies are shown in Figure S4. Using this we obtain two new cylinders centered around the Γ and T points of the BZ. With these cylinders defined, we tessellate them in reciprocal space according to the periodicity of the BZ and then extract the extremal frequencies as would be done for conventional (dHvA or SdH) QOs. The Γ -centred cylinder is a neck and belly cylinder, which along the c -axis will produce frequencies of 8.1 kT and 7.2 kT, whereas the T-centered cylinder will generate frequencies of 3.9 kT and 2.7 kT.

A similar analysis is much more difficult for the 220 T QIO and 4.5 kT breakdown orbit along the a -axis. Instead, we used the analytical form of our Fermi surface model to extract the frequencies. The 220 T QIO results from the interference between quasiparticles moving in the k_z direction on the electron and hole sheets (Figure 5 in the main text). The area corresponding to these oscillations is defined by the warping of the electron cylinder in the k_y direction as it moves away from, and back towards, the hole cylinder. The path of the hole cylinder in k_z as seen from down the a -axis is simply a vertical line, whereas the electron cylinder follows a sinusoidal path in k_y as a function of k_z . The amplitude of the displacement away from the hole cylinder can be defined as :

$$d_y = r_e(1 - \cos(k_z)) \quad (1)$$

where r_e is the degree of warping, which we determine to be $0.006 a_0^{-1}$ from fitting our Fermi surface model [?]. Therefore the area of this loop can be determined as

$$A = \int_{-\pi}^{\pi} r_e(1 - \cos(k_z)) dk_z = 2\pi r_e, \quad (2)$$

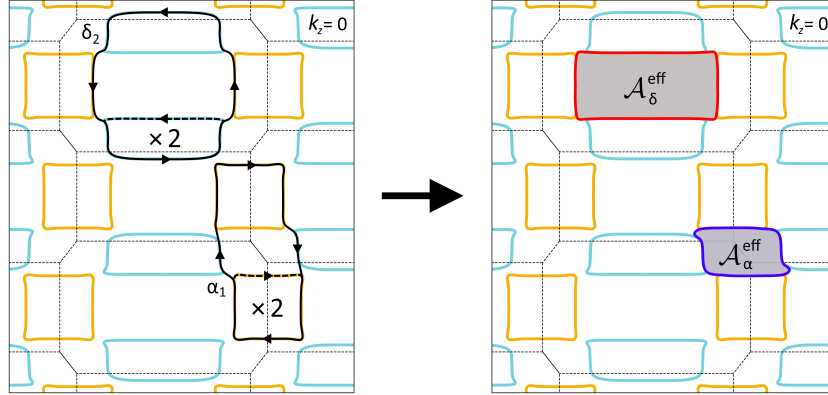


Figure S4: The quantum interference loops responsible for the α and δ frequencies and the corresponding bounding cylinders that were used to calculate their associated frequencies.

which corresponds to a QIO frequency of 206 T, in good agreement with the measured oscillatory frequency.

The larger breakdown orbit can be modelled as an ellipse in the k_y - k_z plane with semi-major axes from $k_z = \pi/c = 0.120 a_0^{-1}$ to $k_z = 0$ and $k_y = 0$ to $k_y = 0.087 a_0^{-1}$ (Figure S5). The area of this orbit corresponds to a frequency of 4.9 kT, in reasonable agreement with the measured frequency of 4.5 kT.

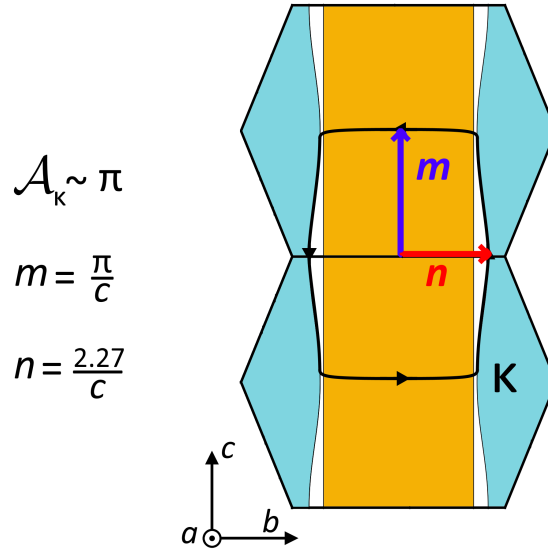


Figure S5: The semi-major axes of the ellipse used to calculate high frequency breakdown orbit, κ , for magnetic field oriented along the a -axis.